Journal of Materials Chemistry C

ESIPT-Suppressed 2-(2'-hydroxyphenyl)benzoxazole derivative as a new photoinitiator for multiphoton polymerization

Journal:	*Journal of Materials Chemistry C*
Manuscript ID	TC-ART-12-2024-005477.R1
Article Type:	Paper
Date Submitted by the Author:	05-Feb-2025

Complete List of Authors:	Valverde, João Victor; Universidade de São Paulo Instituto de Física de São Carlos, Physics and Materials Science Romero, André L.; Universidade de São Paulo Instituto de Física de São Carlos, Physics and Materials Science Cunha, Renan; Universidade de São Paulo Instituto de Física de São Carlos, Physics and Materials Science Garcia, Rafael; Universidade de São Paulo Instituto de Física de São Carlos, Physics and Materials Science Stoerkler, Timothée; Institut de Chimie et Procédés pour l'Énergie l'Environnement et la Santé Massue, Julien; Institut de Chimie et Procedes pour l'Energie l'Environnement et la Sante, Chemistry De Boni, Leonardo; Universidade de São Paulo Instituto de Física de São Carlos, Physics and Materials Science Mendonca, Cleber R.; Universidade de São Paulo Instituto de Física de São Carlos, Physics and Materials Science

ESIPT-Suppressed *2-(2'-hydroxyphenyl)benzoxazole* derivative as a new photoinitiator for multiphoton polymerization

João V. P. Valverde[a], André L. S. Romero[a], Renan Cunha[a], Rafael Q. Garcia[a], Timothée Stoerkler[b], Julien Massue[b], Leonardo De Boni[a] and Cleber R. Mendonça[a,*]

[a] *São Carlos Institute of Physics, University of São Paulo, CP 369, 13560-970 São Carlos, SP, Brazil*
[b] *Institut de Chimie et Procédés pour l'Energie, l'Environnement et la Santé (ICPEES), Université de Strasbourg, UMR CNRS 7515, 67087 Strasbourg Cedex 02, France*

[*] *Author to whom correspondence should be addressed:* crmendon@ifsc.usp.br *and* joaovalverde@ifsc.usb.br

ABSTRACT

The quest for new photoinitiators (PIs) capable of efficiently absorbing multiphoton, particularly three-photon, has intensified due to the multiphoton polymerization (MPP) technique. MPP enables the fabrication of next-generation photonic micro- and nanodevices with resolution beyond the diffraction limit and without shape limitation, offering considerable advantages over other methods. However, designing organic compounds acting as effective multiphoton PI while enabling smart functionalization of manufactured structures remains challenging. In this contribution, we report using a *2-(2'-hydroxyphenyl)benzoxazole* (**HBO**) derivative, named **HBO-NBu$_2$**, as a PI for two- and three-photon polymerization. **HBO** fluorophores are well-known to undergo Excited-State Intramolecular Proton Transfer (ESIPT) process, but in this structure, the combination of a planar and linear *push-pull* dipolar structure, with an extensive π-conjugation, led to a complete suppression of ESIPT, subsequently fulfilling an excellent nonlinear response. Herein, we investigate the linear photophysical properties, excited-state dynamics, and multiphoton absorption of **HBO-NBu$_2$**, supported by quantum chemical calculations. Our results demonstrate that **HBO-NBu$_2$** exhibits structural rigidity, rendering a fluorescence quantum yield of 62% in dichloromethane solution, owing to the absence of ESIPT and substantial intramolecular charge transfer (ICT) due to its *push-pull* nature. Moreover, this molecule shows significant two- and three-photon absorption cross-sections of 80 GM (at 800 nm) and $4 \pm 1 \cdot 10^{-81}\ cm^6\ (s/photon)^2$ (at 1030 nm), respectively. Finally, we demonstrate a proof of concept of MPP using **HBO-NBu2** as PI, showing that even at low concentrations, it outperforms widely used PI.

Keywords: Multiphoton photoinitiator, photopolymerization, two-photon absorption, three-photon absorption, *2-(2'-hydroxyphenyl)benzoxazole* derivative, ESIPT, multiphoton-excited fluorescence technique

1. INTRODUCTION

Material processing using ultrashort laser pulses has become an essential tool in various fields of science and technology, as it enables the development of next-generation micro- and nanophotonic devices. In particular, multiphoton polymerization (MPP) has been widely employed for its ideal characteristics to advance 3D fabrication processes[1,2]. These characteristics derive from the benefits of multiphoton absorption (MPA) processes (two- or three-photon), such as high penetration depth (for wavelengths longer than 800 nm) and high spatial confinement[3,4]. These properties make MPP superior to other fabrication techniques, enabling the creation of 3D structures with subdiffraction-limit resolution, precise dimensional control, and functionalization, reducing undesired thermal or photochemical side reactions[1,5]. In this way, MPP has been employed for the fabrication of high-precision photonic devices, such as microresonators[6], photonic crystals[7], waveguides[8], and smart microenvironments for cell culture[9].

Photopolymerization involves the combination of at least two types of compounds: a monomeric or oligomeric material and a photoinitiator (PI)[10]. Upon light absorption, the PI undergoes a photochemical transformation that generates free radicals, triggering the polymerization process in three steps: initiation, propagation, and termination[2,10]. Thus, successful MPP relies on the use of PIs capable of efficiently absorbing multiphotons (two- or three-photons). In addition to initiating photopolymerization, PIs enable smart functionalization of fabricated structures[1,11], such as embedding *on demand* fluorescent properties to meet specific requirements.

Early studies of MPP included common UV PIs due to their broad commercial availability[5]. However, these PIs exhibit low MPA efficiency[12,13], requiring high excitation intensities and limiting the use of three-photon absorption (3PA), a process that provides higher spatial resolution compared to one- and two-photon absorption (1PA and 2PA), as initially demonstrated by Farsari *et al*.[14] Recent studies have developed organic compounds with strong 2PA and satisfactory performance as two-photon PIs[5,11,15,16]. However, the challenge remains to create viable molecules as three-photon PIs that simultaneously meet specific conditions: efficient 3PA, alignment with the central

wavelengths of widely used femtosecond lasers (Ti:Sapphire and Yb:KGW), and the potential for functionalization of the manufactured structures.

In this context, *2-(2'-hydroxyphenyl)benzoxazole* (**HBO**) derivatives stand out among the various organic compounds because of their straightforward synthesis, chemical and photochemical stability, modularity, and their ability to undergo an Excited State Intramolecular Proton Transfer (ESIPT). ESIPT is a four-level photophysical process occurring in H-bonded organic fluorophores consisting in an excited-state Enol/Keto (E*/K*) tautomerization, translating into a red-shifted tautomeric K* excited species (see **Fig. 1a**)[17,18]. ESIPT derivatives, such as **HBO** dyes, display intrinsic solid-state emission, along with a strong sensitivity to the environment[19]. Indeed, ESIPT can be partially or fully suppressed or even compete with deprotonation, leading to multiple emission profiles, depending on structures and stimuli[20,21]. Recently, we reported the possibility of fully suppressing ESIPT processes by the introduction of ethynyl extension at a selected position as an easy way to provide highly emissive solution-state fluorophores[22], with high energy emissions stemming from the E* state. ESIPT fluorophores act as attractive candidates for a wide range of applications, including laser materials[23], fluorescent probes[24], organic light-emitting diodes[25], and, more recently, two-photon PI for polymerization[15].

Herein, we report the design and use of an **HBO** derivative, named **HBO-NBu$_2$**, as a novel photoinitiator for two- and three-photon polymerization (2PP and 3PP) (see **Fig. 1b**). We synthesized **HBO-NBu$_2$** according to a previously reported procedure[26]. The design includes a *push-pull* dipolar structure (Acceptor-π-Donor) with extensive π-conjugation: the benzoxazole moiety acts as the electron acceptor, the dibutylamide group (**NBu$_2$**) acts as the electron donor, and the ethynyl unit serves as the π-conjugated bridge. This condition meets the specifications set forth by Reinhardt *et al*.[27] and Albota *et al*.[28] for molecules displaying remarkable MPA. **HBO-NBu$_2$** was rationally designed to be ESIPT-inactive owing to a linear delocalization pathway perpendicular to the proton transfer center. As reported before, the electronic transition upon photoexcitation occurs in the π-conjugated spacer, with the hydrogen bond acting as a lock, hindering molecular rotation and promoting higher fluorescence quantum yield (ϕ_{fl})[29]. Furthermore, ESIPT suppression combined with an ethynyl unit (incorporated into the molecular structure) contributes to a highly planar molecular structure favoring MPA.

In this contribution, we conducted a detailed investigation on **HBO-NBu$_2$** linear photophysical properties, complemented by quantum chemical calculations at the DFT

and TD-DFT levels. Moreover, the dynamics of the excited state were analyzed through femtosecond transient absorption spectroscopy and investigate its MPA process (two- and three-photon) using the multiphoton excitation fluorescence (MPEF) technique. Finally, we evaluated the possibility to use **HBO-NBu$_2$** as a PI for MPP, and microstructures with inherent fluorescence emission were manufactured.

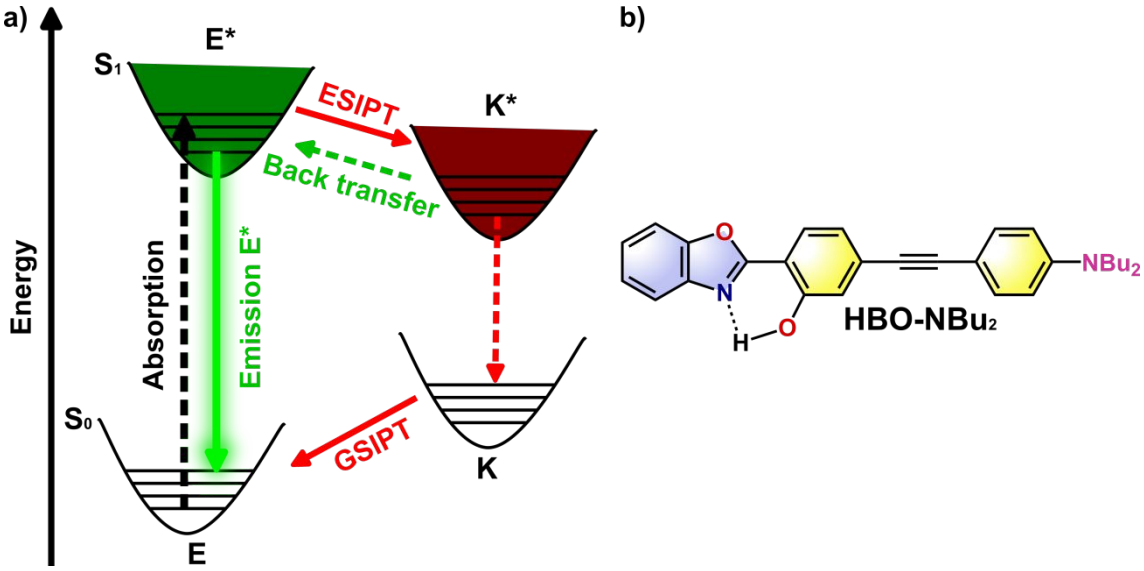

Figure 1 – a) Jablonski diagram illustrating the suppression of the ESIPT process leading to sole E* emission, and b) Molecular structure of **HBO-NBu$_2$**.

2. RESULTS AND DISCUSSIONS

2.1. Linear photophysical properties

Figure 2a (black line) presents the 1PA spectrum of **HBO-NBu$_2$** in dichloromethane (DCM). The compound shows strong absorption in the UV-Vis spectral region, between 250 and 450 nm ($4.96 - 2.76\ eV$). We identified three regions with distinct behaviors, which we associate with three electronic bands. The lowest energy band, located at approximately 394 nm ($3.15\ eV$), exhibits the highest molar absorptivity, with a value of $4.1 \cdot 10^4 M^{-1} cm^{-1}$. The second band, associated with a shoulder is located *ca.* 344 nm ($3.60\ eV$), while the third band is at approximately 307 nm ($4.01\ eV$), with molar absorptivities of $2.0 \cdot 10^4 M^{-1} cm^{-1}$ and $2.5 \cdot 10^4 M^{-1} cm^{-1}$, respectively. We observed that all these transitions are characterized by an intramolecular charge transfer (ICT) process, which is mainly attributed to the typical π-π* transitions in the conjugated backbone of **HBO-NBu$_2$** (*vide infra*)[30,31].

The excitation anisotropy spectrum of **HBO-NBu$_2$** (**Fig. 2b**, black circles) exhibits different patterns depending on the spectral region. Between 375 and 440 nm,

the anisotropy remains almost constant, with an average value of 0.015, indicating that the main absorption band corresponds to a single electronic state, *i.e.*, the S_0-S_1 transition. At wavelengths shorter than 375 nm, the anisotropy sharply decreases until *ca.* 320 nm, suggesting the presence of other states. Below 320 nm, the spectrum exhibits more complex behavior, typical of spectral regions with high electronic state density[32].

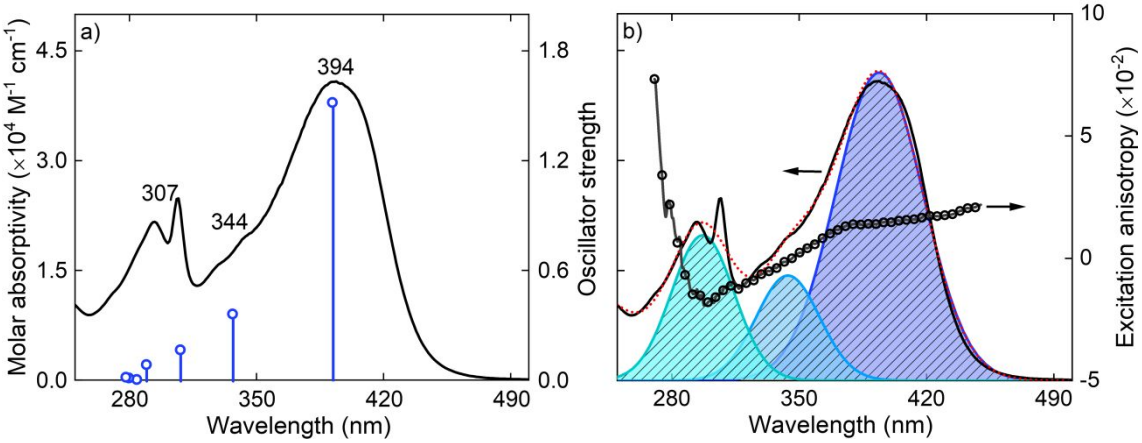

Figure 2 – a) One-photon absorption spectrum (black line: *left axis*) of **HBO-NBu$_2$** in DCM along with oscillator strengths (blue vertical lines: *right axis*) obtained through IEFPCM:TD-B3LYP/6-311++G(d,p) calculations. b) Emission anisotropy spectrum (black circles: *right axis*) and Gaussian decomposition of electronic bands (shaded areas and dashed line is the superposition of Gaussians).

Table 1 – Photophysical properties of **HBO-NBu$_2$** in DCM, including Stokes shift ($\Delta\bar{\nu}_{SS}$), fluorescence lifetime (τ_{fl}), fluorescence quantum yield (ϕ_{fl}), radiative rate (k_r), non-radiative rate (k_{nr}), effective charge displacement length (D_{CT}), transferred charge (q_{CT}), and the difference between the permanent dipole moments of the excited state and the ground one ($|\Delta\vec{\mu}_{01}|$).

Sample	$\Delta\bar{\nu}_{SS}$ (cm^{-1})	τ_{fl} (ns)	ϕ_{fl} (%)	k_r ($\times 10^7 s^{-1}$)	k_{nr} ($\times 10^7 s^{-1}$)	D_{CT} (Å)[a]	q_{CT} ($\|e^-\|$)[a]	$\|\Delta\vec{\mu}_{01}\|$ (D)	
HBO NBu$_2$	5700	2.5 ± 0.4	62 ± 3	25 ± 4	15 ± 4	5.7	0.7	13.5 ± 2[b]	17.5[a]

[a] Quantities obtained through quantum chemical calculations at the IEFPCM:TD-B3LYP/6-311++G(d,p) level.
[b] Quantities obtained through solvatochromism measurement using the Lippert-Mataga equation.

Quantum chemical calculations (QCC) at the PCM-TD-B3LYP/6-311++G(d,p) level have provided us with essential insights into the nature of **HBO-NBu$_2$** electronic bands, especially concerning the highest energy band. As shown in **Fig. 2a** (blue vertical lines), the two lowest energy bands consist of a single electronic transition, corresponding to the S_0-S_1 and S_0-S_2 transitions, which aligns with the anisotropy results. In contrast, the highest energy band is described by multiple electronic transitions, with the S_0-S_3 transition being the most intense. Therefore, the observed behavior agrees with the anisotropy spectrum.

Figure 3a shows the fluorescence emission spectrum of **HBO-NBu$_2$** in DCM, obtained for different excitation wavelengths. The molecule displayed a single

fluorescence emission band in the visible spectral region, with the maximum at *ca.* $508\ nm$ (green), independent of the excitation wavelength. The Stokes shift ($\Delta\bar{\nu}_{SS}$) of approximately $5700\ cm^{-1}$ indicates significant electronic rearrangement in the excited state due to ICT (*vide infra*).

Table 1 summarizes other relevant emissive properties of **HBO-NBu$_2$** in DCM. The molecule exhibits a high ϕ_{fl} of 62% and a relatively long fluorescence lifetime (τ_{fl}) of $2.5\ ns$ (**Fig. 3b**), consistent with values reported for similar compounds[31,33,34]. These results indicate that the main deactivation pathway of the molecule is radiative and validates the absence of ESIPT in **HBO-NBu$_2$**, as ESIPT is usually characterized with low solution ϕ_{fl} in the range $1-5\%$[35]. When comparing the deactivation pathways, one can observe that the radiative rate (k_r) is approximately 1.7 times greater than the non-radiative rate (k_{nr}). While this high ϕ_{fl} is desirable in many applications, some works suggest that it may be unfavorable for photoinitiators, as it can limit the population in the active state required to initiate the photopolymerization process[5,36,37]. However, high ϕ_{fl} is not limiting since it allows us to functionalize the manufactured structures with emissive properties. Also, a high MPA cross-section (σ_{MPA}) can overcome this likely low radical generation efficiency[5].

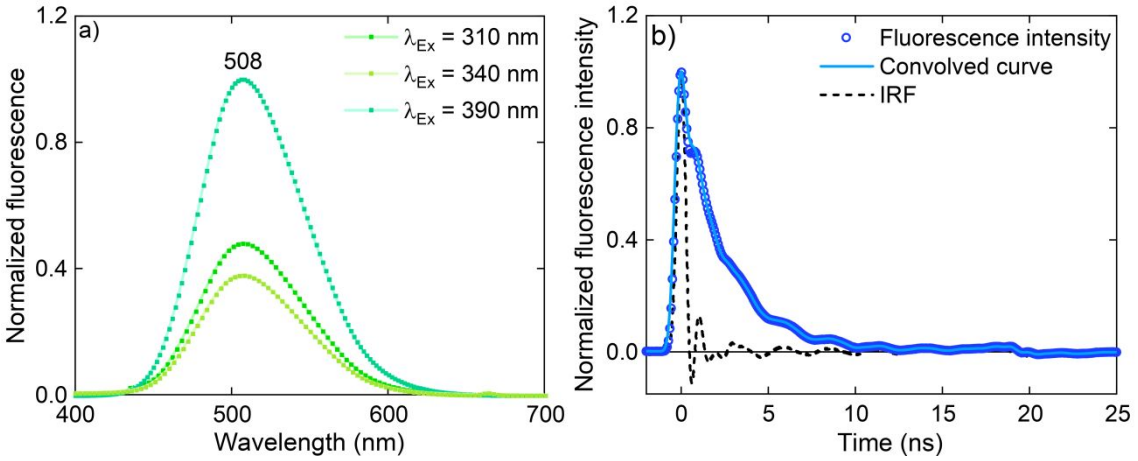

Figure 3 – a) Fluorescence spectrum of **HBO-NBu$_2$** for different excitation wavelengths in DCM. b) Time-resolved fluorescence intensity curve (blue circles), temporal instrument response function (IRF – black dashed line), and the theoretical curve obtained by the convolution method (light blue line).

The highest occupied molecular orbital (HOMO) and lowest unoccupied molecular orbital (LUMO) of **HBO-NBu$_2$**, obtained through QCC, are shown in **Fig. 4a**. The analysis of the orbitals reveals that the electronic excitations HOMO→LUMO, HOMO-1→LUMO, and HOMO-2→LUMO are the ones that best represent the three lowest-energy transitions S_0-S_1, S_0-S_2, and S_0-S_3, respectively. From a qualitative

perspective, one can see that the HOMO and HOMO-1 isodensity surfaces exhibit broad electronic delocalization across the entire conjugated backbone of the molecule. In contrast, the HOMO-2 shows electronic density concentrated until the phenol site, with a negligible contribution from the benzoxazole ring. The LUMO, on the other hand, reveals a redistribution of electronic density, with a reduction in the **NBu_2** unit and an increase near the benzoxazole moiety. We can observe this pattern more clearly in the electron density difference plot depicted in **Fig. 4b**. Therefore, this displays that the electronic excitations (through qualitative analysis) involve a charge transfer between the electron-donating group and the electron-accepting one.

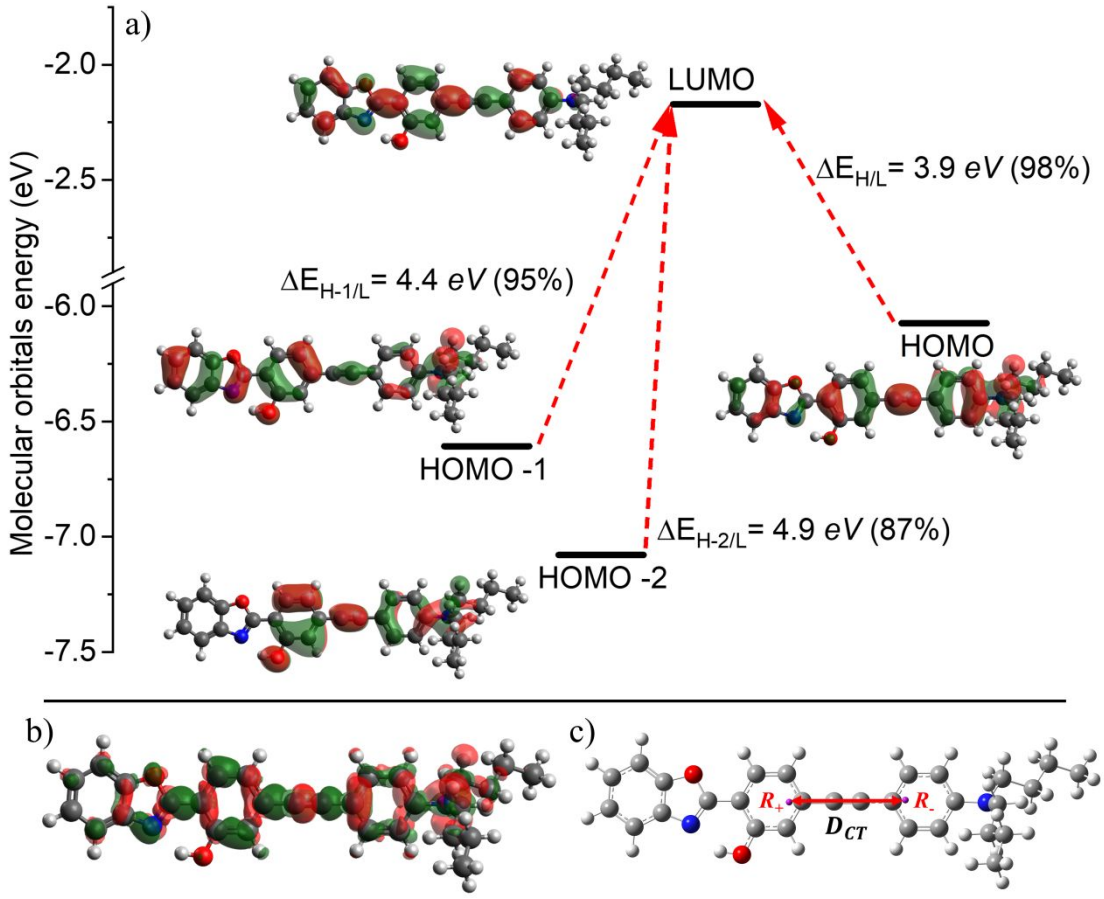

Figure 4 – a) Graphical representation of the molecular orbitals of the **HBO-NBu_2** obtained through QCC at the IEFPCM:TD-B3LYP/6-311++G(d,p) level with the respective energy difference between the orbitals and percentage contribution (contour threshold: $2 \cdot 10^{-2}\ au$). b) Representation of the difference between the excited-state and ground one density (contour threshold: $8 \cdot 10^{-4}\ au$) and c) Barycenter spatial regions of positive (R_+) and negative (R_-) charge.

To quantify the ICT process, we determined the difference between the permanent dipole moment of the excited state and the ground one ($|\Delta\vec{\mu}|$) using the Le Bahers metric and the Lippert-Mataga equation[38–40]. First, **Fig. 4c** shows that the centroids of positive

and negative charge (R_+ and R_-) do not exactly coincide with the electron-donating and -accepting group positions (**NBu_2** and benzoxazole, respectively), showing a displacement relative to them. Nevertheless, the effective charge displacement length (D_{CT}) is 5.7 Å, indicating a considerable separation between the centroids, with a transferred charge (q_{CT}) of 0.7 $|e^-|$. The q_{CT} and D_{CT} values resulted in a $|\Delta\vec{\mu}|$ of 17.5 D. The experimental value of $|\Delta\vec{\mu}|$ obtained by the Lippert-Mataga equation (see **Figs. SI1a**, **SI1b**, and **SI1c**) is $13 \pm 2\ D$: a bit smaller compared to the theoretical one. Despite this slight difference, both results highlight a pronounced ICT character, comparable to that observed in some *push-pull* systems[38,41].

All the above observations highlight the fact that the ESIPT process does not occur in **HBO-NBu_2** and that the observed fluorescence band only stems from the E* state with a strong ICT character. Further on, we provide a more detailed analysis of the excited-state dynamics and present a possible explanation for this behavior.

2.2. Femtosecond transient absorption spectroscopy

We performed femtosecond transient absorption (fs-TA) to investigate the excited-state dynamics of **HBO-NBu_2** in DCM. **Figure 5a** presents a TA signal color map obtained between -1 and 550 ps under 400 nm excitation. The spectrum reveals typical excited-state features in the $450 - 750\ nm$ range (see also **Fig. 5b**). Immediately after the pump pulse, we observed a negative signal at *ca.* $500\ nm$ associated with stimulated emission (SE). We also identified two additional excited-state absorption (ESA) signatures from S_1, at approximately $560\ nm$ and $675\ nm$, with the higher-energy ESA exhibiting the highest absorption amplitude.

Analyzing the TA trace at different delay times, we observed that the higher-energy ESA band undergoes a blue shift of *ca.* $25\ nm$ ($0.11\ eV$, going to *ca.* $535\ nm$) and a reduction in absorption in the first few picoseconds after excitation (**Fig. 5b**). This shift causes significant overlap with the SE band, completely suppressing it. This effect occurs due to the smaller SE cross-section compared to ESA cross-section. We attribute the blue shift to the coaction of two effects: vibrational cooling and solvation[31,42]. Finally, the absorption amplitude remained nearly constant at longer delay times within our observation window.

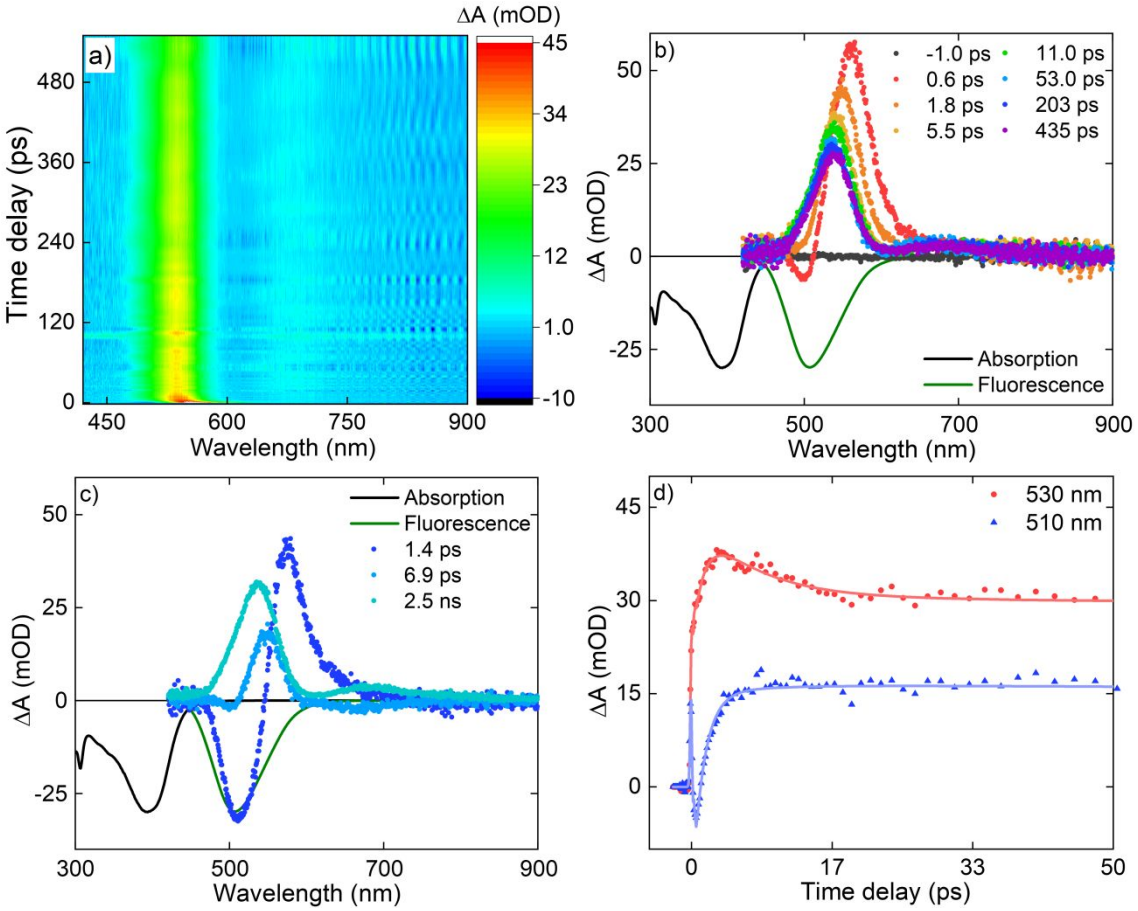

Figure 5 – a) Transient absorption signal color map and b) Transient absorption spectral trace for different delay times, along with absorbance and fluorescence spectra (in arbitrary scale). c) Decay-associated difference spectra of the decay components. d) Transient absorption temporal trace at $530\ nm$ and $510\ nm$.

The data global analysis revealed three spectral components in the decay-associated difference spectra (DADS) (see **Fig. 5c**), with time constants of $1.4\ ps$, $6.9\ ps$, and $2.5\ ns$. As shown in **Fig. 5d**, at the initial instants, the temporal trace at *ca.* $510\ nm$ exhibits rapid growth dynamics with a time constant of $1.4\ ps$, while at $530\ nm$, the decay dynamics occurs on the same timescale. As mentioned earlier, we associate this evolution with vibrational cooling and solvation effects, which is in line with previously described studies[31,42,43]. After the first few picoseconds, one can observe two decay dynamics at $530\ nm$, with time constants of $6.9\ ps$ and $2.5\ ns$. At $510\ nm$, the slower component predominates the dynamics. We attribute the $6.9\ ps$ time constant to the process of structural relaxation of the molecule in the excited state, while the $2.5\ ns$ component, whose DADS spectrum resembles the TA spectrum, corresponds to the excited-state lifetime, which, in this case, is the same as τ_{fl}. Furthermore, the absence of sub-picosecond dynamics ($0.3 - 0.6\ ps$) corroborates the assumption that the **HBO-NBu$_2$** does not undergo ESIPT process[30,44–46].

To better understand this behavior, we analyzed the charge density plot in **Fig. 4b**, which revealed that after electronic excitation, an increase in charge density is observed on the heterocyclic *nitrogen* atom, making it more basic in the excited state. In contrast, the hydroxyl group exhibits only a small green lobe, suggesting that its acidity does not drastically change in the excited state. This behavior contrasts with what we observe in typical ESIPT systems. Munch *et al*.[33] conducted a thorough study on a series of benzazoles similar to **HBO-NBu$_2$**. They demonstrated that, in the **HBO** series, the hydroxyl group acidity remains almost unchanged during the electronic transition in DCM, resulting in the complete suppression of the ESIPT process in this series, which is in agreement with our observation. We attribute this suppression to the functionalization of the **HBO** core at the *meta* position relative to the hydroxyl group, resulting in a less centered electronic delocalization in the core ESIPT and, consequently, disfavors proton transfer. Indeed, Massue *et al*.[47] and Xu *et al*.[48] demonstrate that functionalizing the **HBO** core at the *para* position (relative to the hydroxyl group) promotes the ESIPT process. Furthermore, in linear *push-pull* systems such as **HBO-NBu$_2$**, ESIPT can be fine-tuned by modifying the nature of the heterocycle — replacing the oxygen atom with nitrogen or sulfur — and adjusting the strength of the electron-donating group[33].

Our results highlight several key points about **HBO-NBu$_2$**. In the excited state, the molecule undergoes significant ICT. Due to the extended π-conjugation, the electronic delocalization in the excited state is less centered on the ESIPT core, disfavoring the proton transfer process. Consequently, we observe solely the enol excited state (E* transition). This behavior can also influence the pathway for the generation of radicals. Durko-Maciag *et al*.[15] suggest that radicals in their **HBO** derivatives form in the excited keto K* state. By extrapolating this hypothesis to **HBO-NBu$_2$**, we can expect radical formation to occur in the enol-excited state without needing a prior ESIPT process.

2.3. Multiphoton absorption and multiphoton photopolymerization

Figure 6a presents the 1- and 2PA spectra of **HBO-NBu$_2$**. We determined σ_{2PA} in the range of 500 to 900 nm, while σ_{3PA} was measured at 1030 nm, employing the absolute MPEF technique. The analysis of the fluorescence intensity dependence versus the excitation power (**Fig. 6b**) reveals slopes of 2.1 ± 0.2 and 2.9 ± 0.3 on a logarithmic scale for excitation at 800 nm and 1030 nm, respectively, confirming the 2- and 3PA nature. The good agreement between the fluorescence emission spectrum

obtained from multiphoton and one-photon excitation, as evidenced in the inset of **Fig. 6b**, confirms the pure nature of the fluorescence.

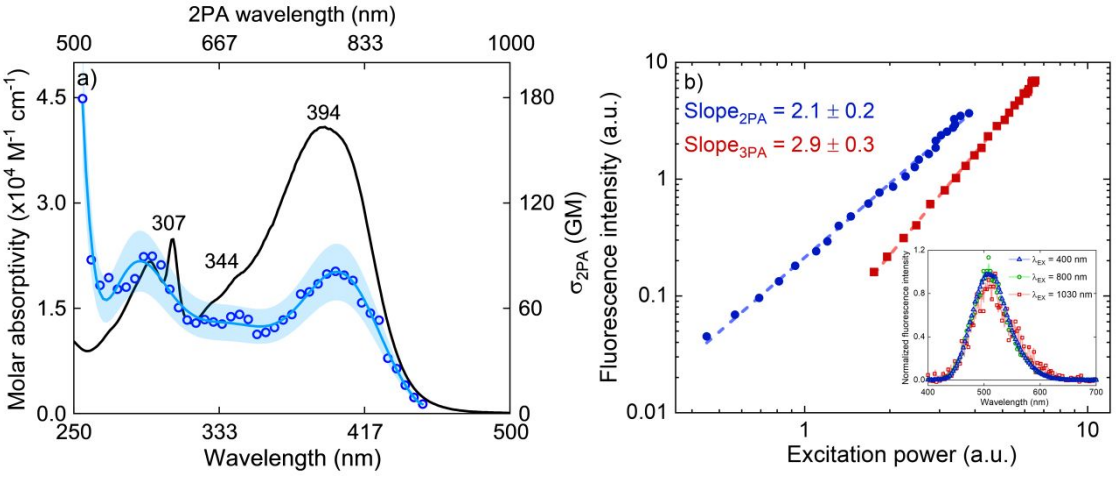

Figure 6 – 2PA (blue circles: *right and top axis*) and 1PA (black line: *left and bottom axis*) spectra of the **HBO-NBu$_2$** molecule in DCM. The light blue line is a visual guide, while the light blue hatched area represents the error dispersion of approximately 20%. b) Fluorescence emission signal as a function of excitation power (log-log scale). The blue dots and red squares represent excitation at 800 and 1030 nm, respectively. The dashed lines are the linear fit. The inset in b) displays the fluorescence emission spectrum obtained for excitation at 400, 800, and 1030 nm.

The 2PA spectrum exhibits a spectral structure very similar to the 1PA one, which can be attributed to the relaxation of the dipole selection rule due to the Acceptor-π-Donor dipolar structure[49]. We observed the highest σ_{2PA} at *ca.* 590 and 790 nm, with values of approximately 90 ± 20 GM and 80 ± 20 GM, respectively. For excitation at 1030 nm, σ_{3PA} was $(4 \pm 1) \cdot 10^{-81}\, cm^6\,(s/photon)^2$ (see **Table 2**). These results indicate a considerable nonlinear response of **HBO-NBu$_2$**, which we attribute to its significant ICT and high structural planarity, that leads to an increase in its polarizability. It is worth highlighting that the MPA of the molecule aligns well with the central wavelengths of two widely used femtosecond laser generations: Ti:Sapphire and Yb:KGW. This alignment makes the **HBO-NBu$_2$** even more promising for practical applications.

Table 2 – Nonlinear photophysical properties of **HBO-NBu$_2$** and other photoinitiators. The presented properties include the solvent used, the 2PA cross-section (σ^{2PA}) at different excitation wavelengths, and the 3PA cross-section (σ^{3PA}) at 1030 nm.

Sample	solvent	σ^{2PA}_{530} $(GM)^*$	σ^{2PA}_{800} $(GM)^*$	σ^{3PA}_{1030} $\left(\times 10^{-81} cm^6 (s/photon)^2\right)$
HBO-NBu$_2$	DCM	70 ± 10	80 ± 20	4 ± 1
Lucirin TPO-L[a]	Ethanol[a]	n.d.	0.05[a]	n.d.
Irgacure OXE01[b]	Methanol[b]	n.d.	2.8[b]	n.d.
ITX[b]	Methanol[b]	n.d.	1.9[b]	n.d.

BDEBP[c]	1-propanol[c]	n.d.	6.0[c]	n.d.
DEDC[d]	trichloromethane[d]	n.d.	29.5[d]	n.d.

$* \ 1\ GM = 1 \cdot 10^{-50} cm^4 s/photon$. [a, b, c, and d] Previously reported by Mendonça *et al.*[50], Schafer *et al.*[12], Nazir *et al.*[51], and Li *et al.*[13], respectively.

Comparing the results obtained for **HBO-NBu$_2$** with those from other studies, we observed that its σ_{2PA} is comparable to that of various PIs. For instance, common UV PIs exhibit σ_{2PA} values ranging from 0.05 to 29.5 GM at 800 nm (see **Table 2**). These results indicate that **HBO-NBu$_2$** displays a 2PA that is, on average, 10 times higher than these UV PIs. Compared with compounds of the same class as **HBO-NBu$_2$**, Durko-Maciag *et al.*[15] reported maximum values between 2.3 to 26 GM for HBO-based photoinitiators at 532 nm, within the region of higher 2PA; this would yield much smaller values at 800 nm. In a study by Otuka *et al.*[11], the authors reported σ_{2PA} ranging from 47 to 750 GM at 790 nm for azoaromatic-based PIs. However, it is worth highlighting that 750 GM values are in the region of resonant enhancement and do not represent pure 2PA processes. It is worth mentioning recent studies in which quadrupolar and octapolar molecules are specially designed to exhibit a high σ_{2PA}, reaching hundreds of GM at 800 nm[5,52].

After determining the MPA of the **HBO-NBu$_2$**, we investigated its efficiency as a two- and three-photon PI. There are various methods to evaluate the efficiency of PIs; in this study, we chose to fabricate 3D structures and, from that, determine the 2PP threshold fluence for different concentrations of **HBO-NBu$_2$**, in a mixture with two acrylic resins, *ethoxylated(6)trimethylolpropane triacrylate* (SR499 – Sartomer) and *tris(2-hydroxyethyl)isocyanurate triacrylate* (SR368 – Sartomer) (**Fig. SI2**), employed in equal mass proportions. We define the threshold fluence as the minimum energy required to initiate the photopolymerization process. For 3PP, we investigated the process only at the maximum concentration.

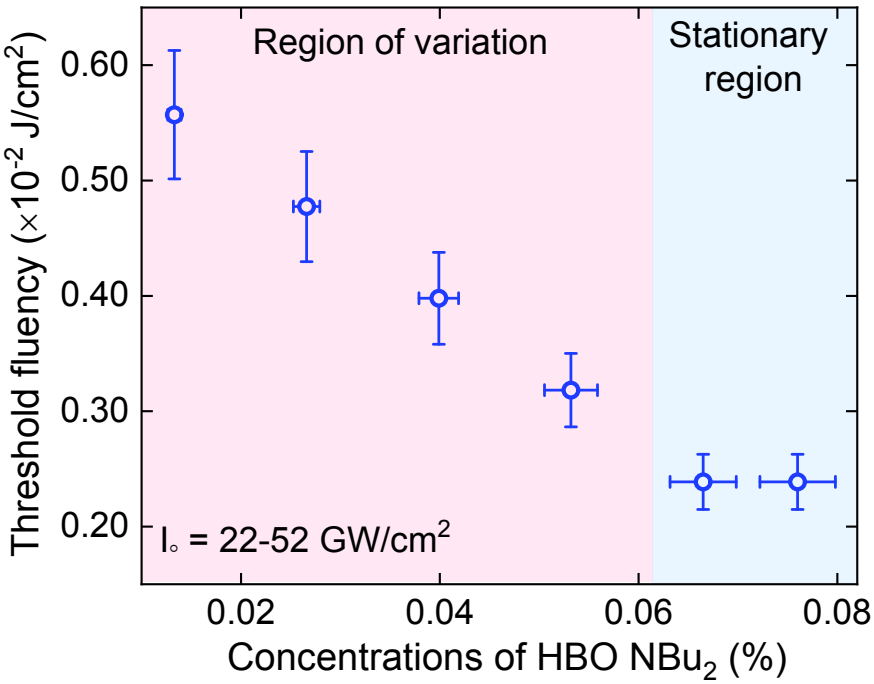

Figure 7 – Threshold fluence curve versus the mass concentration of the **HBO-NBu₂** molecule ($wt\%$) mixed with acrylic resins. The shaded area indicates different behaviors of the threshold fluence curve. $I_\circ$ represents the peak intensity range used.

In **Fig. 7**, we present the threshold fluence ranging from 0.002 to 0.006 J/cm^2 (0.075 to 0.18 nJ) for different concentrations of **HBO-NBu₂**, which we used in the range between 0.01 and 0.08 $wt\%$. The threshold fluence curve displays two distinct regions. The first region, characterized by an almost linear behavior, shows that the threshold fluence rapidly decreases as the concentration of **HBO-NBu₂** increases, up to approximately 0.05 $wt\%$. In the second region, we observe a threshold fluence saturation at $0.024\,J/cm^2$, regardless of further concentration increases ($0.07 - 0.08\,wt\%$). Regarding 3PP, we observed that the threshold fluence at maximum concentration was approximately $0.20\,J/cm^2$ ($6.0\,nJ$).

Comparing our results of 2PP to HBO-based photoinitiators, we observed that **HBO-NBu₂** can initiate photopolymerization with 4800 times lower energy per pulse and 38 times lower concentration[15]. The difference is less pronounced for azoaromatic-based photoinitiators, with **HBO-NBu₂** requiring 8 times lower energy per pulse and 12 times lower concentration[11]. Finally, compared to the photoinitiator Lucirin TPO-L, a highly efficient UV compound, the energy per pulse becomes similar, although Lucirin TPO-L requires a 38 times higher concentration[53]. Regarding 3PP, the first demonstration employed an organic-inorganic hybrid platform and showed excellent 3PP capability[14]. Although the scope of the study was not on the relation between the PI concentration and

3PP threshold, the authors showed polymerized high-resolution structures with 7.5 less energy per pulse than in our work. This result indicates a notable efficiency of **HBO-NBu$_2$** as a two- and three-photon PI, even at low concentrations, aligning with the central wavelengths of widely used femtosecond lasers (Ti:Sapphire and Yb:KGW).

Finally, **Fig. 8** shows images of the microfabricated structures using 2PP and 3PP. The qualitative analysis reveals the high quality of these structures, allowing us to fabricate lines with a resolution of up to $560\ nm$ (**Figure 8d**). We believe achieving even smaller resolution is possible, as Farsari *et al.*[14] demonstrated through 3PP. Due to the high ϕ_{fl} of **HBO-NBu$_2$**, only a fraction of molecules forms free radicals, consequently initiating photopolymerization. The remaining molecules preserve their photophysical properties (within the fabricated structure), which gives the microfabricated structures an intrinsic fluorescence emission, as observed in the confocal fluorescence microscopy shown in **Fig. 8e-g**.

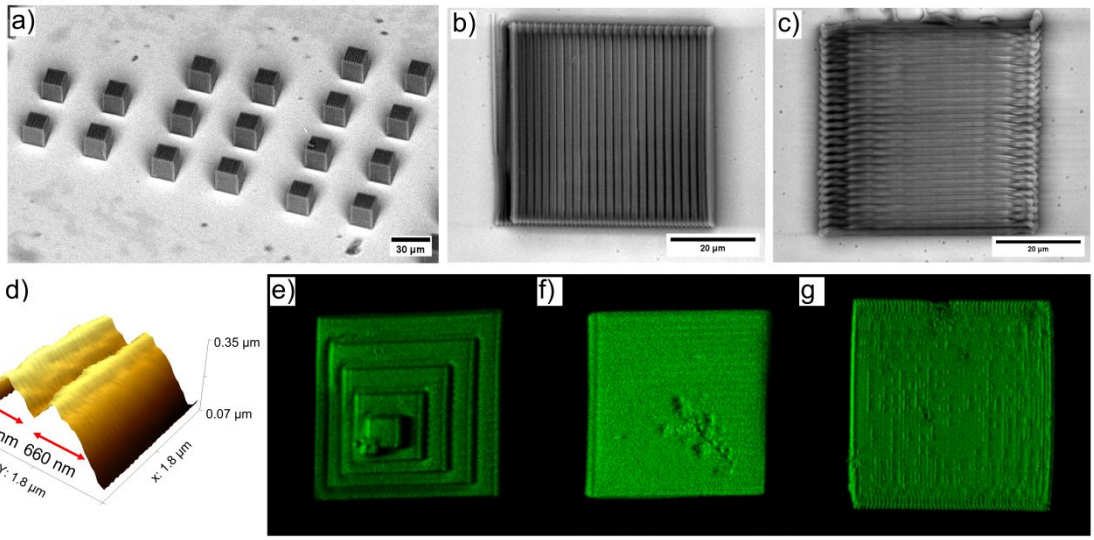

Figure 8 – Scanning electron microscopy images of the microstructures fabricated by a,b) 2PP and c) 3PP. d) Atomic force microscopy image of the microstructure by 2PP, whose profile trace showed an FWHM of 460 and 660 nm. Confocal fluorescence microscopy image (excitation beam at $440\ nm$) of the microstructures d-e) from 2PP and f) from 3PP.

3. CONCLUSION

In summary, we determined the linear photophysical properties, excited-state dynamics, and multiphoton absorption process of **HBO-NBu$_2$** in DCM. We obtained σ_{2PA} and σ_{3PA} using MPEF techniques, while fs-TA spectroscopy allowed us to investigate the excited-state dynamics. Finally, based on the significant absorption cross-section values obtained, we evaluated the suitability of **HBO-NBu$_2$** as a PI for MPP.

We demonstrated that **HBO-NBu$_2$** exhibits strong 1PA in the range of $250-450\,nm$, consistent with the results from QCC. The molecule presents fluorescence emission at $508\,nm$, with a ϕ_{fl} of 62% and a τ_{fl} of $2.5\,ns$. We observed a considerable Stokes shift attributed to substantial ICT in the excited state, as indicated by $|\Delta\vec{\mu}_{01}|$. The dynamics of the excited state revealed two fast time constants associated with vibrational cooling, solvation, and structural relaxation processes. We did not identify any sub-picosecond time scale components, indicating that the ESIPT process in the excited state of **HBO-NBu$_2$** is entirely suppressed despite a strong intramolecular hydrogen bond ($H-O\cdots N$). In this context, the hydrogen bond acts as a lock, which, along with the ethynyl unit, provides high planarity to the molecular structure, positively impacting the dynamics of the excited state and the MPA process. The **HBO-NBu$_2$** molecule exhibits σ_{2PA} and σ_{3PA} of $80\,GM$ $(790\,nm)$ and $4 \pm 1 \cdot 10^{-81}\,cm^6\,(s/photon)^2$ $(1030\,nm)$, respectively, surpassing the values observed in widely used UV PIs. Finally, we confirmed the viability of **HBO-NBu$_2$** as a PI for 2PP and 3PP by fabricating microstructures with inherent emissive properties. Overall, these findings establish the **HBO-NBu$_2$** molecule as a promising PI for MPP, highlighting its exceptional photophysical properties and potential for advanced applications in microfabrication.

4. EXPERIMENTAL DETAILS

In the *Supplementary Information* (**SI**) section, we describe all the details about the measurements performed, the equipment used, and the procedures for the quantum chemical calculations.

Supporting information description

Section SI1 describes the procedures for measuring linear photophysical properties, including one-photon absorption, fluorescence emission, fluorescence quantum yield, solvatochromism, and excitation anisotropy. In **SI2**, we detail the multiphoton-excited fluorescence technique to measure two- and three-photon absorption. **SI3** presents the femtosecond transient absorption technique, while **SI4** covers fluorescence lifetime measurement. In **SI5**, we address the quantum chemical calculation procedures and the results obtained, such as equilibrium geometry and

electronic transition properties. Finally, **SI6** describes the methodology and procedures for multiphoton polymerization, and **SI7** lists the references.

Corresponding author

João Victor Pereira Valverde – Instituto de Física de São Carlos, Universidade de São Paulo, São Carlos, SP, 13560-970, Brasil. Orcid: https://orcid.org/0000-0003-3611-0597. E-mail: joaovalverde@ifsc.usp.br.

Cleber R. Mendonça – Instituto de Física de São Carlos, Universidade de São Paulo, São Carlos, SP, 13560-970, Brasil. Orcid: https://orcid.org/0000-0001-6672-2186. E-mail: crmendon@ifsc.usp.br.

Credit authorship contribution statement

João Victor P. Valverde: Conceptualization, Methodology, Project Administration, Investigation, Data Curation, Formal Analysis, Visualization, Software, Validation, Writing – Original Draft.

André Luis S. Romero: Conceptualization, Methodology, Investigation, Data Curation, Validation, Writing – Review & Editing.

Renan Cunha: Conceptualization, Methodology, Investigation, Data Curation, Validation, Writing – Review & Editing.

Rafael Q. Garcia: Conceptualization, Methodology, Investigation, Software, Data Curation, Validation, Writing – Review & Editing.

Timothée Stoerkler: Conceptualization, Methodology, Resources, Validation, Writing – Review & Editing.

Julien Massue: Conceptualization, Methodology, Resources, Validation, Visualization, Writing – Review & Editing.

Leonardo De Boni: Conceptualization, Methodology, Project Administration, Supervision, Funding Acquisition, Resources, Data Curation, Validation, Writing – Review & Editing.

Cleber Renato Mendonça: Conceptualization, Methodology, Project Administration, Supervision, Funding Acquisition, Resources, Data Curation, Validation, Writing – Review & Editing.

Declaration of competing interest

The authors declare that they have no known competing financial interests or personal relationships that could have appeared to influence the work reported in this paper.

Data availability

The authors confirm that the data supporting the conclusions of this study are available in the article and its **SI**.

ACKNOWLEDGMENTS

Financial support from FAPESP (Fundação de Amparo à Pesquisa do Estado de São Paulo, grants 2016/20886–1, 2018/11283–7, and 2024/12541-0, CNPq (Conselho Nacional de Desenvolvimento Científico e Tecnológico), Coordenação de Aperfeiçoamento de Pessoal de Nível Superior (CAPES) - Finance Code 001, Air Force Office of Scientific Research (FA9550-23-1-0664), and Army Research Laboratory (W911NF-21-1-0362).

REFERENCES

1 A. J. G. Otuka, N. B. Tomazio, K. T. Paula and C. R. Mendonça, *Polymers (Basel)*, DOI:10.3390/polym13121994.

2 X. Zhou, Y. Hou and J. Lin, *AIP Adv*, DOI:10.1063/1.4916886.

3 M. Pawlicki, H. A. Collins, R. G. Denning and H. L. Anderson, 2009, preprint, DOI: 10.1002/anie.200805257.

4 K. D. Belfield, S. Yao and M. V. Bondar, 2008, preprint, DOI: 10.1007/12_2007_126.

5 Z. Li, N. Pucher, K. Cicha, J. Torgersen, S. C. Ligon, A. Ajami, W. Husinsky, A. Rosspeintner, E. Vauthey, S. Naumov, T. Scherzer, J. Stampfl and R. Liska, *Macromolecules*, 2013, **46**, 352–361.

6 N. B. Tomazio, A. J. G. Otuka, G. F. B. Almeida, X. Roselló-Mechó, M. V. Andrés and C. R. Mendonça, *J Polym Sci B Polym Phys*, 2017, **55**, 569–574.

7 G. von Freymann, A. Ledermann, M. Thiel, I. Staude, S. Essig, K. Busch and M. Wegener, *Adv Funct Mater*, 2010, **20**, 1038–1052.

8 S. Klein, A. Barsella, H. Leblond, H. Bulou, A. Fort, C. Andraud, G. Lemercier, J. C. Mulatier and K. Dorkenoo, *Appl Phys Lett*, DOI:10.1063/1.1915525.

9 P. Tayalia, C. R. Mendonca, T. Baldacchini, D. J. Mooney and E. Mazur, *Advanced Materials*, 2008, **20**, 4494–4498.

10 S. O'Halloran, A. Pandit, A. Heise and A. Kellett, *John Wiley and Sons Inc*, 2023, preprint, DOI: 10.1002/advs.202204072.

11 A. J. G. Otuka, B. B. M. Torres, J. Dipold, D. T. Balogh, V. Tribuzi, L. De Boni and C. R. Mendonça, *Opt Mater Express*, 2020, **10**, 1792.

12 K. J. Schafer, J. M. Hales, M. Balu, K. D. Belfield, E. W. Van Stryland and D. J. Hagan, *J Photochem Photobiol A Chem*, 2004, **162**, 497–502.

13 C. Li, L. Luo, S. Wang, W. Huang, Q. Gong, Y. Yang and S. Feng, *Two-photon microstructure-polymerization initiated by a coumarin derivative/iodonium salt system*, .

14 M. Farsari, G. Filippidis and C. Fotakis, *Fabrication of three-dimensional structures by three-photon polymerization*, 2005.

15 M. Durko-Maciag, G. Ulrich, J. Massue, J. Mysliwiec and K. Cyprych, *Eur Polym J*, DOI:10.1016/j.eurpolymj.2023.112235.

16 X. Cao, F. Jin, Y. F. Li, W. Q. Chen, X. M. Duan and L. M. Yang, *New Journal of Chemistry*, 2009, **33**, 1578–1582.

17 J. Massue, D. Jacquemin and G. Ulrich, *Chem Lett*, 2018, **47**, 1083–1089.

18 J. Zhao, S. Ji, Y. Chen, H. Guo and P. Yang, *Phys. Chem. Chem. Phys.*, 2012, **14**, 8803–8817.

19 M. Durko-Maciag, G. Ulrich, D. Jacquemin, J. Mysliwiec and J. Massue, *Physical Chemistry Chemical Physics*, 2023, **25**, 15085–15098.

20 T. Stoerkler, G. Ulrich, P. Retailleau, S. Achelle, A. D. Laurent, D. Jacquemin and J. Massue, *Chemistry – A European Journal*, DOI:10.1002/chem.202402448.

21 T. Stoerkler, G. Ulrich, P. Retailleau, A. D. Laurent, D. Jacquemin and J. Massue, *Chem Sci*, 2024, **15**, 7206–7218.

22 M. Munch, E. Colombain, T. Stoerkler, P. M. Vérité, D. Jacquemin, G. Ulrich and J. Massue, *J Phys Chem B*, 2022, **126**, 2108–2118.

23 C. Rullière and J. Joussot-Dubien, *Opt Commun*, 1978, **24**, 38–40.

24 K. Tanaka, T. Kumagai, H. Aoki, M. Deguchi and S. Iwata, *J Org Chem*, 2001, **66**, 7328–7333.

25 C.-W. Ko, Y.-T. Tao, A. Danel, L. Krzemińska and P. Tomasik, *Chemistry of Materials*, 2001, **13**, 2441–2446.

26 J. Massue, D. Frath, P. Retailleau, G. Ulrich and R. Ziessel, *Chemistry – A European Journal*, 2013, **19**, 5375–5386.

27 B. A. Reinhardt, L. L. Brott, S. J. Clarson, A. G. Dillard, J. C. Bhatt, R. Kannan, L. Yuan, G. S. He and P. N. Prasad, *Highly Active Two-Photon Dyes: Design, Synthesis, and Characterization toward Application*, 1998.

28 M. Albota, D. Beljonne, J.-L. Brédas, J. E. Ehrlich, J.-Y. Fu, A. A. Heikal, S. E. Hess, T. Kogej, M. D. Levin, S. R. Marder, D. Mccord-Maughon, J. W. Perry, H. Röckel, M. Rumi,

G. Subramaniam, W. W. Webb, X.-L. Wu and C. Xu, *Design of Organic Molecules with Large Two-Photon Absorption Cross Sections*, 1998, vol. 281.

29 M. Raoui, J. Massue, C. Azarias, D. Jacquemin and G. Ulrich, *Chemical Communications*, 2016, **52**, 9216–9219.

30 Y. Li, X. Bai, R. Liang, X. Zhang, Y. H. Nguyen, B. VanVeller, L. Du and D. L. Phillips, *Journal of Physical Chemistry B*, 2021, **125**, 12981–12989.

31 N. Alarcos, M. Gutierrez, M. Liras, F. Sánchez and A. Douhal, *Physical Chemistry Chemical Physics*, 2015, **17**, 16257–16269.

32 W. V. Moreshead, O. V. Przhonska, M. V. Bondar, A. D. Kachkovski, I. H. Nayyar, A. E. Masunov, A. W. Woodward and K. D. Belfield, *Journal of Physical Chemistry C*, 2013, **117**, 23133–23147.

33 M. Munch, E. Colombain, T. Stoerkler, P. M. Vérité, D. Jacquemin, G. Ulrich and J. Massue, *Journal of Physical Chemistry B*, 2022, **126**, 2108–2118.

34 M. Serhan, M. Sprowls, D. Jackemeyer, M. Long, I. D. Perez, W. Maret, N. Tao and E. Forzani, in *AIChE Annual Meeting, Conference Proceedings*, American Institute of Chemical Engineers, 2019, vol. 2019- November.

35 T. Stoerkler, T. Pariat, A. D. Laurent, D. Jacquemin, G. Ulrich and J. Massue, *European J Org Chem*, DOI:10.1002/ejoc.202200661.

36 T. Wloka, S. Czich, F. Chalupa-Gantner, M. Sittig, M. Dirauf, C. Weber, M. Gottschaldt, K. Liefeith, A. Ovsianikov, B. Dietzek-Ivanšić and U. S. Schubert, *J Photochem Photobiol A Chem*, DOI:10.1016/j.jphotochem.2023.114743.

37 J. F. Xing, W. Q. Chen, X. Z. Dong, T. Tanaka, X. Y. Fang, X. M. Duan and S. Kawata, *J Photochem Photobiol A Chem*, 2007, **189**, 398–404.

38 T. Le Bahers, C. Adamo and I. Ciofini, *J Chem Theory Comput*, 2011, **7**, 2498–2506.

39 N. Mataga, Y. Kaifu and M. Koizumi, *Bull Chem Soc Jpn*, 1956, **29**, 465–470.

40 E. Lippert, *Zeitschrift für Elektrochemie, Berichte der Bunsengesellschaft für physikalische Chemie*, 1957, **61**, 962–975.

41 I. Ciofini, T. Le Bahers, C. Adamo, F. Odobel and D. Jacquemin, *Journal of Physical Chemistry C*, 2012, **116**, 11946–11955.

42 C. R. Hall, J. Conyard, I. A. Heisler, G. Jones, J. Frost, W. R. Browne, B. L. Feringa and S. R. Meech, *J Am Chem Soc*, 2017, **139**, 7408–7414.

43 E. Gomez, N. Alarcos, C. Monterde, F. Sánchez, M. Moreno and A. Douhal, *Physical Chemistry Chemical Physics*, 2018, **20**, 27149–27161.

44 B. Gierczyk, S. S. Murphree, M. F. Rode and G. Burdzinski, *Sci Rep*, DOI:10.1038/s41598-022-23759-9.

45 J. Xie, Z. Wang, R. Zhu, J. Jiang, T.-C. Weng, Y. Ren, S. Han, Y. Huang and W. Liu, DOI:10.3390/ijms.

46 Q. J. Meisner, J. J. M. Hurley, P. Guo, A. R. Blood, R. D. Schaller, D. J. Gosztola, G. P. Wiederrecht and L. Zhu, *Journal of Physical Chemistry A*, 2022, **126**, 1033–1061.

47 J. Massue, G. Ulrich and R. Ziessel, *European J Org Chem*, 2013, **2013**, 5701–5709.

48 L. Xu, Q. Wang and Y. Zhang, *Dyes and Pigments*, 2017, **136**, 732–741.

49 K. D. Bonin, T. J. Mcllrath, K. D. Bonin and T. J. Mcilrath, *Two-photon electric-dipole selection rules*, 1984, vol. 1.

50 C. R. Mendonca, D. S. Correa, T. Baldacchini, P. Tayalia and E. Mazur, *Appl Phys A Mater Sci Process*, 2008, **90**, 633–636.

51 R. Nazir, P. Danilevicius, A. I. Ciuciu, M. Chatzinikolaidou, D. Gray, L. Flamigni, M. Farsari and D. T. Gryko, *Chemistry of Materials*, 2014, **26**, 3175–3184.

52 C. Arnoux, T. Konishi, E. Van Elslande, E. A. Poutougnigni, J. C. Mulatier, L. Khrouz, C. Bucher, E. Dumont, K. Kamada, C. Andraud, P. Baldeck, A. Banyasz and C. Monnereau, *Macromolecules*, 2020, **53**, 9264–9278.

53 T. Baldacchini, C. N. LaFratta, R. A. Farrer, M. C. Teich, B. E. A. Saleh, M. J. Naughton and J. T. Fourkas, *J Appl Phys*, 2004, **95**, 6072–6076.

DATA AVAILABILITY STATEMENT

The authors confirm that the data supporting the conclusions of this study are available in the article and its **SI**.